



Effect of cytochrome *c* on the phase behavior of charged multicomponent lipid membranes



Salome Pataria^a, Yonggang Liu^{a,b}, Reinhard Lipowsky^a, Rumiana Dimova^{a,*}

^a Department of Theory and Bio-Systems, Max Planck Institute of Colloids and Interfaces, Science Park Golm, 14424 Potsdam, Germany

^b State Key Laboratory of Polymer Physics and Chemistry, Changchun Institute of Applied Chemistry, Chinese Academy of Sciences, 130022 Changchun, China

ARTICLE INFO

Article history:

Received 9 December 2013

Received in revised form 14 April 2014

Accepted 18 April 2014

Available online 26 April 2014

Keywords:

Giant vesicles

Phase diagram (Gibbs triangle)

Egg sphingomyelin

DOPG

Cholesterol

Confocal microscopy

ABSTRACT

We studied the effect of submicromolar concentrations of cytochrome *c* (cyt *c*) on the phase behavior of ternary lipid membranes composed of charged dioleoylphosphatidylglycerol, egg sphingomyelin and cholesterol. The protein was found to induce micron-sized domains in membranes belonging to the single-fluid-phase region of the protein-free ternary mixture and, as a result, to expand the region of coexistence of liquid ordered (L_o) and liquid disordered (L_d) phases. Direct observations on individual vesicles revealed that protein adsorption increases the area of L_d domains. Measurements using a fluorescent analog of cyt *c* showed that the protein preferentially adsorbs onto domains belonging to the L_d phase. The adsorption was quantitatively characterized in terms of partitioning ratios between the L_d and the L_o phases. The protein was also found to induce vesicle leakage even at relatively low concentrations. In eukaryotic cells under normal physiological conditions, cyt *c* is localized within the intermembrane space of mitochondria. During cell apoptosis, cyt *c* is released into the cytosol and its adsorption to intracellular membranes may strongly perturb the lipid distribution within these membranes as suggested by our results.

© 2014 Elsevier B.V. All rights reserved.

1. Introduction

Interactions of water-soluble proteins with membranes play an important role in many biological processes, such as signal transduction and transport processes [1]. A good example for such a water-soluble protein is the peripheral membrane protein cytochrome *c* (cyt *c*), which is a globular heme protein with a diameter of about 3.4 nm, carrying approximately 4 effective positive charges. With its well characterized structure and many important biological functions, cyt *c* is a suitable model macromolecule for studying the association and interaction of peripheral proteins with lipid membranes.

In general, upon adsorption to a membrane composed of negatively charged and neutral lipids, a peripheral positively charged protein may induce local changes in lipid composition. A number of theoretical studies have considered this problem, see e.g. [2,3], but experimental evidence for adsorption-induced lipid demixing is rather limited. Mainly single- and two-component lipid membranes in the presence of cyt *c* have been studied [4–11]. The role of protein adsorption on the stability of liquid ordered and liquid disordered phases in membranes has not been addressed in detail.

Lipid rafts have been proposed as functionally important components of cell membranes. A number of studies indicate their involvement in processes such as protein and lipid sorting and signal

transduction, cholesterol transport, membrane trafficking, cytoskeleton adhesion, fusion and fission, endocytosis and apoptosis; see e.g. references [12–18]. A new development in molecular medicine called “membrane-lipid therapy” relies on the interaction of proteins with lipid domains to modulate the cell activity, thus providing a possible treatment of human diseases [19,20]. Because of the resolution limitations of optical microscopy, it is difficult to detect nanometer-sized membrane domains enriched in saturated lipids, cholesterol and specific proteins, and the existence of such domains in living cells still a matter of debate [21]. On the other hand, model systems such as giant unilamellar vesicles (GUVs) [22,23] containing cholesterol and sphingolipids can serve as a powerful tool to visualize raft-like liquid ordered domains for characterizing biologically relevant phenomena; see e.g. references [24–28]. In membranes composed of mixtures of saturated and unsaturated lipids with cholesterol at room temperature, one can observe phase separation and domain formation on the micron scale. Depending on the membrane composition and with the help of fluorescently labeled lipids, one can then visualize domains in GUVs by confocal microscopy [29]. Recently, it has been demonstrated that phase separation and domain formation can be visualized not only in membranes containing mixtures of zwitterionic lipids but also for ternary mixtures with anionic lipids [30–32], which in turn opens new possibilities for investigating systems relevant to biological membranes. In particular, the inner leaflet of the plasma membrane as well as the membranes of many cellular organelles which have been proposed to exhibit raft-like domains contain charged lipids [33–35]. The

* Corresponding author. Tel.: +49 331 5679615; fax: +49 331 5679612.
E-mail address: Rumiana.Dimova@mpikg.mpg.de (R. Dimova).

mitochondrial membrane also contains a number of charged lipids, such as phosphatidylinositols, fatty acids and cardiolipin, whose total fraction is of the order of a few tens weight percent [36].

In this work, we used cyt *c* as a model protein to address the effect of adsorption of a positively charged protein to negatively charged membranes with several fluid domains. The latter membranes contained both zwitterionic and anionic lipids. The interaction of cyt *c* with these lipids involves a number of different factors. Several studies indicate that the peripheral or integral binding of cyt *c* to charged lipid membranes depends on the lipid-to-protein (L/P) molar ratio. It has been shown that for low L/P ratios below approximately 8, horse heart cyt *c* binds electrostatically to pure dioleoylphosphatidylglycerol (DOPG) vesicles, whereas at higher L/P ratios above approximately 18, partial penetration of cyt *c* into the lipid bilayer takes place [4]. Furthermore, the adsorption of cyt *c* to negatively charged lipid membranes is highly dependent on the ionic strength of the solutions. On the one hand, at low ionic strength and high (horse heart) cyt *c* concentrations, the protein might even insert into DOPG lipid bilayers [5,6]. On the other hand, binding of cyt *c* to membranes containing a fraction of the charged lipid cardiolipin, was shown to weaken in solutions of low ionic strength. Collapse of cardiolipin-rich domains was also observed [7]. Binding of cyt *c* to single-component membranes composed of anionic lipids also leads to changes in the phase behavior of the lipids: Upon binding, cyt *c* lowers the phase transition temperature and broadens the transition of charged phosphatidylglycerol lipids [8]. Lateral lipid redistribution of two-component membranes made of anionic and neutral lipids has also been observed; see e.g. [9–11] and references therein. Large micrometer-sized domains in phosphatidylcholine vesicles containing a small fraction of phosphatidic acid were detected [9]. However, the effect of cyt *c* on the phase state of membranes with more complex lipid composition exhibiting phase separation has not been explored so far.

In this study, the interaction of yeast cyt *c* with three-component lipid membranes was investigated by measuring the changes in the phase behavior of these membranes. The preferential partitioning of cyt *c* between different membrane domains was quantitatively characterized as well as the change in the domain area fractions upon adsorption of the protein. GUVs composed of the mixture DOPG, egg sphingomyelin (eSM) and cholesterol (Chol) were used as a model system, where DOPG is a negatively charged unsaturated lipid, mimicking the lipid environment of cyt *c* in the cell. Indeed, phosphatidylglycerol (PG) was chosen as a mimic for the charged lipids in the mitochondrial membrane because of its relatively low pK_a (around 3). The low pK_a implies that PGs remain charged in unbuffered or weakly buffered solutions even when local effects caused by salt or changes in the lipid environment are taken into account [37,38]. Furthermore, PGs are used as a precursor for cardiolipin synthesis in the inner membrane of mitochondria [39] and can substitute for cardiolipin in a number of mitochondrial functions [40]. Cholesterol and saturated lipids are also present in mitochondrial membranes, with a larger fraction in the outer mitochondrial membrane [36].

We characterized the phase diagram of the ternary mixture DOPG/eSM/Chol in the absence and presence of cyt *c* using confocal microscopy to image the GUVs. Changes in the domain areas and vesicle leakage upon cyt *c* adsorption to phase separated membranes were investigated. The partitioning of cyt *c* between liquid-disordered and liquid-ordered domains was quantitatively determined and the role of the overall membrane composition explored.

2. Materials and methods

2.1. Materials

The lipids DOPG (1,2-dioleoyl-*sn*-glycero-3-phospho-[1'-rac-glycerol], sodium salt), eSM and cholesterol were purchased from Avanti Polar Lipids (Alabaster, AL). The fluorescent labels 1,1'-dioctadecyl-3,3,3',3'-tetramethylindocarbocyanine perchlorate (DiIC₁₈)

and 1,2-distearoyl-*sn*-glycero-3-phosphoethanolamine-N-[poly(ethylene glycol) 2000-N'-carboxyfluorescein] (DSPE-PEG2000-CF) were obtained from Molecular Probes (Eugene, OR) and Avanti Polar Lipids, respectively. Yeast cyt *c* (*Saccharomyces cerevisiae*), HEPES (4-(2-hydroxyethyl)-1-piperazineethanesulfonic acid) and EDTA (ethylenediaminetetraacetic acid disodium salt dehydrate) were purchased from Sigma Aldrich (Steinheim, Germany). Alexa Fluor 633 carboxylic acid succinimidyl ester for fluorescent labeling of cyt *c* was purchased from Invitrogen (Darmstadt, Germany). Labeling was performed according to the protocol of the manufacturer. The final concentration of the fluorescently labeled protein was checked with UV/VIS spectroscopy.

2.2. Vesicle formation

GUVs composed of DOPG/eSM/Chol mixtures were prepared by the method of electroformation [41] with some modifications [30]. Briefly, 10 μ l of 2 mg/ml of the lipid mixture in chloroform was spread on conductive glasses coated with indium tin oxide (ITO). The lipid mixtures contained 0.4 mol.% of the fluorescent dyes DiIC₁₈ and/or DSPE-PEG2000-CF. In order to remove the organic solvent, the ITO glasses were dried at 60 °C under high vacuum for 2 h. A chamber was formed by inserting a rectangular Teflon spacer between two opposing ITO coated glasses with the conductive sides facing each other. About 2 ml of preheated 100 mM sucrose solution in a 2 mM HEPES/1 mM EDTA buffer at pH 7.5 was injected into the chamber. In the following, we will refer to the 2 mM HEPES/1 mM EDTA buffer at pH 7.5 simply as to the buffer. The chamber was then placed in an oven at 60 °C. An AC field with amplitude of 1.0 V (peak-to-peak) and frequency of 10 Hz was applied for 2 h. Afterwards, the chamber was removed from the oven and left at room temperature (~23 °C) for equilibration. The vesicle suspension was then diluted with a solution of 110 mM glucose in buffer at room temperature.

2.3. Confocal laser scanning microscopy

The GUV solution was placed in a sealed chamber, and the top-view vesicle observation was done by Leica TCS SP5 confocal microscope (Heidelberg GmbH, Germany) with a 63 \times water immersion objective. The dyes DiIC₁₈ and DSPE-PEG2000-CF were excited with a diode-pumped solid-state laser at 561 nm and an argon laser at 488 nm, respectively. The emission signals were collected separately in the ranges 571–671 nm and 500–600 nm, respectively. To reduce artifacts due to light-induced domain formation [42,43] illumination with low intensity of the laser source was used.

Fluorescently labeled yeast cyt *c* stock solution at a concentration of 7.4 μ M was prepared in buffer. The glass slides of the observation chamber were pretreated with unlabeled cyt *c* solution at a concentration of 4 mM to avoid vesicle adhesion and bursting. After coating, the glass slides were rinsed with distilled water and dried. This step also ensured that there is no protein loss due to adhesion of the positively charged cyt *c* to the negatively charged glass walls of the chamber. After introducing the GUV suspension, the protein solution was added drop-wise up to a final protein concentration of 0.56 μ M. Samples were left for at least 30 min to ensure that the adsorption of protein to the vesicles has reached equilibrium; see Fig. S1 in the Supporting Information. Yeast cyt *c* was excited with a laser source of 633 nm and fluorescence emission was collected between 642 nm and 720 nm. Bleaching of the protein dye within the typical observation times was not detected; see Fig. S2 in the Supporting Information.

2.4. UV/VIS spectroscopy

A Helios Gamma UV/VIS spectrophotometer (Fisher Scientific GmbH, Germany) was used to measure the absorbance spectra of the unlabeled yeast cyt *c* in quartz cuvettes with a path length of 1 cm. The absorption was measured at concentrations between 1 and 5 μ M

in buffer for the wavelength range of 300–600 nm. The spectra were used to determine the extinction coefficient of cyt *c* at 410 nm.

2.5. Flow chamber measurements

A flow chamber made in house was used for single vesicle observation to resolve changes in the domain area fraction before and after the addition of cyt *c*. The flow chamber consisted of a nylon frame with holes on both sides connected to Tygon tubing for fluid exchange. The nylon frame was sealed from above and below with glass slides using silicone grease. The chamber was carefully filled with buffer avoiding bubble formation. Then the vesicle solution was introduced. The chamber was left to rest for approximately 40 min to allow for the vesicles to settle at the chamber bottom. Afterwards, the cyt *c* solution was injected into the system with a programmable VIT-FIT syringe pump (LAMBDA CZ s.r.o., Czech Republic) at sufficiently low speed that did not disturb the system by fluid flow and allowed to monitor a selected vesicle. The amount of the introduced cyt *c* solution exceeded the chamber volume 4 times. Then the system was left to equilibrate for a minimum of 30 min. During the injection and resting time, the vesicles were observed with phase contrast using laser illumination at 633 nm to avoid artifacts associated with oxidation of the fluorescent dye. The 3D images were recorded with bidirectional scanning using the DPSS laser at 561 nm.

3. Results and discussion

3.1. Phase diagram of the ternary mixture DOPG/eSM/Chol

We characterized GUVs composed of DOPG, which represents an unsaturated lipid with a low melting temperature carrying a net negative

charge, eSM, a high melting temperature lipid, and cholesterol. The transition temperature of DOPG is $-18\text{ }^\circ\text{C}$. Thus, at room temperature, this lipid is in the fluid phase. At room temperature, eSM is still in the gel phase and enters the fluid phase only at $39\text{ }^\circ\text{C}$. Thus, at room temperature membranes composed of the DOPG/eSM/Chol mixture can exhibit immiscibility depending on the specific membrane composition. This was already demonstrated in a previous study, where vesicles made of this mixture and in glucose/sucrose solutions were shown to exhibit phase separation and domain formation depending on the particular membrane composition [30]; see inset in Fig. 1 for data on the phase state of DOPG/eSM/Chol vesicles in buffer-free solution. To provide protein-friendly conditions with pH control, here we investigated the phase behavior of this ternary mixture in a 2 mM HEPES/1 mM EDTA buffer at pH 7.5, which is typically used for studies involving cyt *c*. It is known that the phase state of membranes is sensitive to small changes in the environment, e.g., in pH, temperature or ions [44]. As we will show below, indeed the presence of the buffer results in a number of changes in the phase diagram of the DOPG/eSM/Chol mixture, compared to the phase diagram of the same mixture in buffer-free solution.

Confocal microscopy was used to explore in detail more than 70 different membrane compositions in the Gibbs triangle of the DOPG/eSM/Chol mixture in buffer at room temperature ($\sim 23\text{ }^\circ\text{C}$) after an equilibration time of approximately 2 h. Our first aim was to locate the coexistence region of liquid ordered (L_o) and liquid disordered (L_d) phases, which is biologically relevant [45]. The fluorescently labeled lipid DiI₁₈ used in our studies is known to preferentially partition into the L_d phase and to be excluded from L_o and solid ordered (S) domains [46]. The marker DSPE-PEG2000-CF preferentially partitions into the L_o phase. Our measurements suggested that it is sufficient to use only the dye DiI₁₈ in order to characterize the phase diagram of DOPG/eSM/Chol from confocal images of GUVs. The following domain features

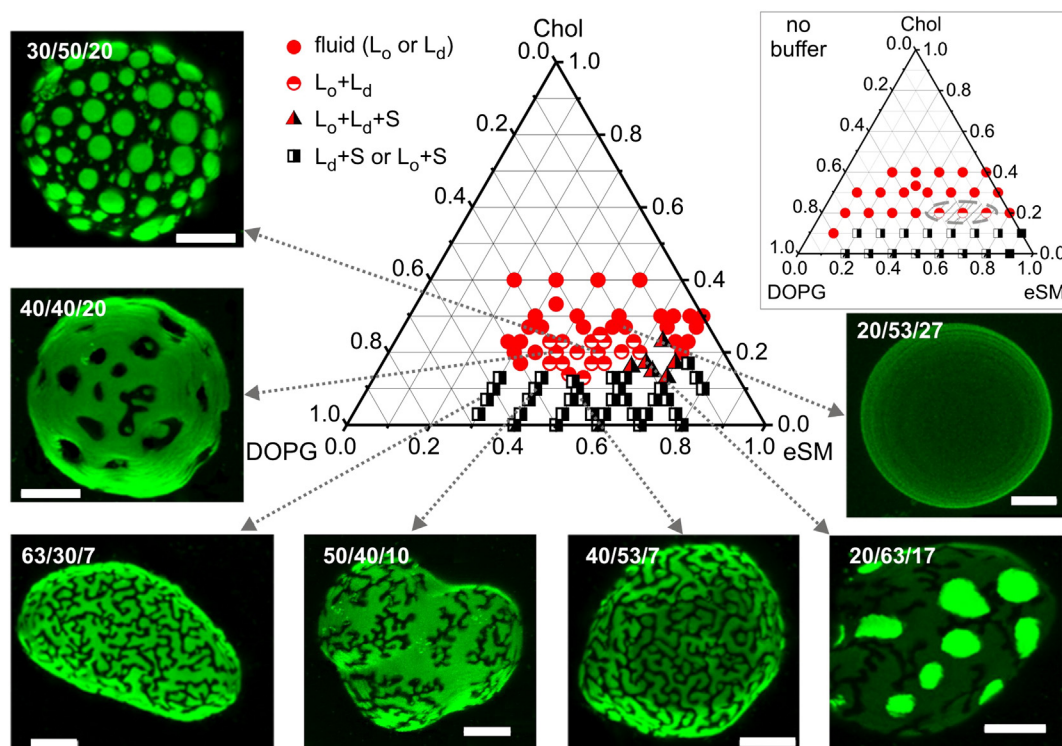


Fig. 1. Phase diagram of the DOPG/eSM/Chol ternary mixture obtained from confocal laser scanning microscopy observations on GUVs at $(23 \pm 1)\text{ }^\circ\text{C}$. The GUV solutions used were 100 mM sucrose (inside)/110 mM glucose solution (outside) in 2 mM HEPES/1 mM EDTA buffer at pH 7.5. The vesicles were labeled with DiI₁₈ (green false color) which partitions preferentially into the L_d phase. The images, representing 3D projections, were used to identify different phase regions in the Gibbs triangle; see text for details. For clarity, only single vesicle halves are shown. One should note that the domain patterns for L_o – L_d coexistence as shown for the composition 30/50/20 represent transient patterns after about 20 minutes. Full equilibration takes about two hours and always leads to a final pattern with only two large domains as in Fig. 3A. For comparison, the inset in the upper right part shows the phase diagram of DOPG/eSM/Chol in buffer-free sugar solutions as obtained in Ref. [30]. The different symbols correspond to the notation in the main legend. The hatched area in the inset indicates the region of L_o – L_d phase coexistence. Scale bars represent 10 μm .

were used to distinguish the various regions in the Gibbs triangle. For vesicles in the single-fluid-phase (L_o or L_d) region, the fluorescent dye is homogeneously distributed in the membrane and the vesicles appear smooth, quasispherical and with fluctuating membrane; see vesicle image corresponding to the composition 20/53/27 DOPG/eSM/Chol in Fig. 1. In the region of coexistence of the two fluid phases L_o and L_d , the domains have smooth boundaries and are free to move relative to each other; see images with compositions 30/50/20 and 40/40/20 in Fig. 1. These two images display transient domain patterns with many small and large domains as observed after about 20 min. Full equilibration takes about 2 h and eventually leads to complete phase separation with one L_o and one L_d domain as one would expect theoretically [47]. When one fluid phase and the gel phase (L_d and S or L_o and S) coexist, the solid domains are depleted from fluorescent dye and appear dark, exhibit angular features and are rigid with fixed boundaries; see images with compositions 63/30/7, 50/40/10 and 40/53/7 in Fig. 1. These vesicles may also appear faceted. For GUVs with a composition in the three-phase coexistence region (L_d , L_o and S), three types of domains can be distinguished: (i) angular, rigid and very dark S domains; (ii) weakly fluorescent L_o domains and (iii) strongly fluorescent L_d domains; see image with composition 20/63/17 in Fig. 1. All confocal snapshots of GUVs were made in 3D projection; for the compositions in the fluid phase, only one vesicle hemisphere was captured to avoid artificial deformation in the images caused by membrane fluctuations. For some of the compositions examined, and in particular for those that are close to the boundaries of the coexistence regions, we observed both vesicles with and without domains. This phase variation in the vesicle composition arises from the preparation method and has also been observed in earlier studies [30,48–51]. The overall membrane phase state shown in Fig. 1 corresponds to a “majority rule”, i.e., more than 50% of the vesicles were in this particular phase state. Between 70 and 100 vesicles per batch were examined and for some of the compositions, in particular those close to the phase boundaries, several batches were prepared and studied.

Based on these observations, we were able to partially construct the phase diagram of DOPG/eSM/Chol in buffer; see Fig. 1. Compared to the conditions of buffer-free glucose/sucrose solutions as in reference [30], see inset in Fig. 1, we observe that the coexistence region of two fluid phases (L_d and L_o) is slightly shifted towards higher DOPG concentrations, and, in addition, expanded in this direction. Furthermore, we detect a three-phase coexistence region (L_d , L_o and S), see triangular data points in Fig. 1 and the associated image in the lower right corner of Fig. 1.

The differences in the media surrounding the membrane in the two studies consist of the following: In reference [30], the investigated vesicles were in 0.2 M glucose solution. Here, the vesicles were prepared in 0.1 M glucose but in addition to this, we used a buffer of 1 mM EDTA and 2 mM HEPES at pH 7.5. Thus, the study in Ref. [30] and that in the present paper differ in the pH and the ionic strengths of the aqueous solutions. For the 0.2 M glucose solution, we measured a pH of 6.1 and a conductivity of 1.8 mS/m, whereas the conductivity of the buffered glucose solution at pH 7.5 was found to be 25.7 mS/m, i.e., more than tenfold higher. The small difference in the pH has presumably a negligible effect. The higher ionic strength of the buffered solution, however, could explain the observed changes in the phase diagram. Addition of salts, i.e. increased ionic strength, was already shown to stabilize the two-phase coexistence region of this ternary mixture, as expressed in an increase in the miscibility temperature [30].

3.2. Effect of cyt c on the phase behavior of the DOPG/eSM/Chol ternary mixture

After characterizing the phase diagram of the DOPG/eSM/Chol ternary mixture in buffer, we studied the influence of cyt c on the membrane phase behavior. Cyt c is known to influence the main phase transition of single-component PG membranes by broadening

as well as lowering the gel-to-liquid-crystal phase transition temperature [8,52]. In two-component membranes made of anionic and neutral lipids, cyt c was observed to induce lateral lipid redistribution [9–11] and, in some cases, formation of large micrometer-sized domains [9].

For the majority of our observations, we chose a protein concentration of 0.56 μM in order to characterize the changes in the phase diagram of the ternary lipid mixture (other protein concentrations were also explored as discussed later in the text). The vesicles were observed for approximately 30 min after adding the protein solution to allow for a homogeneous distribution of cyt c in the chamber and equilibration of the adsorption process; see Fig. S1 in the Supporting Information. The observations were up to 1 h after mixing to avoid possible domain-induced budding, in particular, for membrane compositions close to the binodal of the two-fluid-phase coexistence region. After adding the cyt c to the solution, the domains appeared to be symmetric across the bilayer, i.e., the domains in one leaflet appeared to be in registration with domains in the opposite leaflet, as observed for symmetric membranes [53].

First, we considered compositions within the two-fluid-phase coexistence ($L_d + L_o$) region. Upon the addition of cyt c, changes in the domain sizes were observed (see next section for details) without, however, changing the phase state ($L_d + L_o$). We then explored vesicles with composition from the single-fluid-phase region (L_d or L_o). In this case, for certain membrane compositions, cyt c induced phase separation and formation of fluid domains. This result is consistent with previous observations studying the changes in the membrane phase state and domain formation in DOPG/eSM/Chol upon contact with positively charged large unilamellar vesicles [30]. We also examined lipid compositions from the solid-fluid ($L_d + S$, $L_o + S$ and $L_d + L_o + S$) coexistence regions. In particular, we explored the mixtures 60/30/10, 50/40/10, 40/50/10 DOPG/eSM/Chol. In these solid-fluid coexistence regions of the phase diagram, cyt c was not observed to alter the phase state of the membrane, namely, the vesicles continued to exhibit coexisting solid and fluid domains (we did not determine possible changes in the domain area fraction caused by cyt c). Presumably, the inter-lipid cohesive interactions in the gel phase are strong enough to prevent protein-induced rearrangement of the lipids and demixing.

Fig. 2 summarizes the results describing the changes in the phase state of DOPG/eSM/Chol membranes upon interaction with cyt c at a

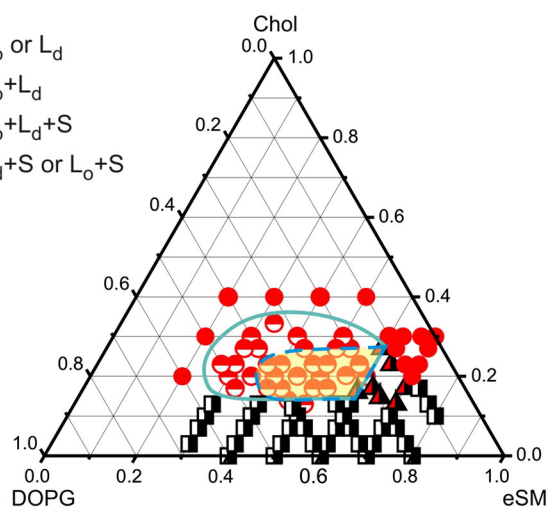


Fig. 2. Changes in the phase diagram of DOPG/eSM/Chol membranes in buffer in the presence of 0.56 μM cyt c at $(23 \pm 1)^\circ\text{C}$. The solid blue curves represent the putative boundaries of the coexistence region for liquid-ordered and liquid-disordered phases. The area shaded in light yellow and outlined with the blue dashed curve represents the two-fluid-phase coexistence region in the absence of cyt c as displayed in Fig. 1. This area is expanded in the presence of cyt c. No changes in the membrane phases were detected for the other compositions. Because of the inherent variation in the vesicle composition, all outlined coexistence regions should be considered as rough guides to the eye.

concentration of 0.56 μM . The region of two-fluid-phase coexistence is enlarged at the expense of the single-fluid-phase region; see the blue boundary of the phase coexistence region in Fig. 2. Thus, we conclude that the adsorption of cyt *c* leads to an extension or enlargement of the L_d – L_o coexistence region. In the absence and presence of cyt *c*, the estimated L_d – L_o phase boundary is given by the broken blue curve and the solid blue curve in Fig. 2, respectively.

Because the phase boundaries were deduced from optical microscopy, one could imagine that the formation of micron-sized domains within the new cyt *c*-induced extension of the L_d – L_o coexistence region arises from the coalescence of submicron domains that exist already in the absence of cyt *c*. However, such a scenario is rather unlikely because, in the absence of cyt *c*, the deduced L_d – L_o coexistence region corresponds to complete phase separation characterized by the formation of two large domains after an equilibration time of about 2 h. Therefore, we would need a molecular mechanism that stabilizes the submicron domains and prevents their coalescence within the extension of the L_d – L_o coexistence region but is ineffective within the original L_d – L_o coexistence region of the protein-free system. Such a mechanism is hard to imagine because this mechanism would apply, for any chosen tie-line, only to some segment of this tie-line, even though the material parameters characterizing the two membrane domains have constant values along the whole tie-line. On the other hand, one could speculate that local segregation and molecular clustering in the membrane are initiated upon adsorption of cyt *c*, which would induce the formation of L_d and L_o domains in regions of the phase diagram where only single (L_o or L_d) phases are observed in the absence of the protein.

As mentioned in the introduction, the effect of cyt *c* on the membrane depends on the lipid-to-protein (L/P) molar ratio in the system. Thus, we expected that the vesicle response should depend on the overall protein concentration. We investigated the phase state changes in DOPG/eSM/Chol vesicles brought into contact with solutions of cyt *c* at various concentrations in the range from 1 nM to 1.39 μM . At very low concentrations, 6.5 nM and lower, no changes in the phase state of the membranes in the one-fluid-phase region were detected under the microscope (membranes with the following compositions were monitored: 50/30/20, 40/30/30 and 30/40/30). At very high protein concentrations, 1.2 μM and higher, the changes induced on the membrane phase state were difficult to characterize because the vesicles appeared unstable upon adding the protein solution and ruptured in a bursting fashion or collapsed in a way similar to events reported for cardiolipin doped membranes [7]. (Note that these protein concentrations are comparable to typical lipid concentrations in GUV systems.) For intermediate concentrations, we observed changes associated with the phase state of the membrane (as illustrated by the phase diagram in Fig. 2 for a cyt *c* concentration of 0.56 μM) and changes in the domain sizes for membrane compositions belonging to the region of two-fluid-phase coexistence.

Several studies in the literature have explored the effect of factors such as the L/P ratio and the ionic strength on the mode of interaction of cyt *c* with the membrane. Thus, we estimated the L/P ratio for our system at a protein concentration of 0.56 μM . For this purpose, we assumed that there was no lipid loss during the preparation of the vesicles and their transfer to the observation chamber. If we consider the total lipid and not only the external leaflet of the membrane immediately accessible to cyt *c* in the bulk, the L/P ratio is approximately 16. For such an L/P ratio and low ionic strength of the solution (as in our system), the predominant protein–membrane interactions are of electrostatic nature [4]. Let us note however, that the studies in reference [4] have been performed on pure DOPG vesicles, while in our system, the fraction of DOPG in the membrane is lower and varies. In addition, we cannot fully exclude the possibility that cyt *c* interacts with eSM, for which studies are not available in the literature to the best of our knowledge. Thus, interactions of non-electrostatic nature cannot be entirely excluded.

3.3. Changes in the domain areas upon binding of cyt *c*

We evaluated the area change of fluid domains upon adsorption of cyt *c* using a flow chamber to introduce the protein at a concentration of 0.56 μM . We used two ways of monitoring the domain area changes, both of which have advantages and disadvantages: (i) We selected a vesicle and directly followed the changes upon introducing the protein solution. Such experiments are laborious because of the long observation times and the difficulty of following a single vesicle during the exchange of solutions in the observation chamber. Thus, only a few vesicles per membrane composition were observed. (ii) We examined a population of vesicles before introducing cyt *c*, and then investigated another vesicle population after adding the protein. The advantage of in this approach is that the results are statistically averaged over many vesicles. However, the history of the individual vesicles is not known and frequent vesicle budding during the solution exchange, leading to systematic shifts in the vesicle compositions, is to be expected. In both approaches, there are concerns about the exact membrane composition of the vesicles. It is known that for multicomponent lipid mixtures, the composition of vesicles in a batch can vary drastically from vesicle to vesicle depending on the individual vesicle history during the preparation step. Particularly strong deviations in the vesicle composition are observed for multicomponent lipid mixtures which are not fully miscible at the temperature of observation [30,48,51]. One important advantage of the first approach, however, is that each explored vesicle has the same initial and final lipid composition, whereas studies of vesicle populations involve averages over different components.

Below, we present results using both approaches. The vesicles were labeled with DiI_{C18} which partitions into the L_d phase. For the area measurements, we chose spherical vesicles exhibiting only two domains. Apart from being well equilibrated (the phase separation and domain coalescence are completed), calculating the domain areas in such vesicles is simple. The domains have the shapes of spherical caps and the domain area can be estimated from measurements of the projected domain diameter and the vesicle radius.

We chose to examine three different membrane compositions which exhibit two-fluid-phase (L_d/L_o) coexistence in the absence of cyt *c*: 20/60/20, 30/50/20 and 40/40/20; see also Fig. 6B. The cardiolipin concentration in the inner membrane of mitochondria ranges from 18% to 24% of the lipid content [36]. Taking into account that cardiolipin possesses two negative charges compared to PG, which carries only one net charge, the compositions we have chosen are a suitable mimic for the mitochondrial membrane in terms of the membrane surface charge.

Fig. 3A gives an example for the behavior of a single vesicle upon addition of cyt *c*. The membrane composition is 30/50/20 DOPG/eSM/Chol. The initial area fraction of the L_d domain is $(21.05 \pm 0.75)\%$ and, after the addition of the protein solution, it increases to $(26.12 \pm 0.70)\%$. The error represents standard deviation from image processing. Measurements on two other vesicles with this membrane composition yielded change by 7.31% and 1.75%. The sizes of the vesicles were not observed to change. Observations on three other vesicles made of 40/40/20 and 20/60/20 DOPG/eSM/Chol yielded similar changes in the L_d domain area fraction, namely an increase between 3 and 5%. No dependence on the area increase as a function of the membrane composition was observed. Statistical measurements over populations of vesicles made of 30/50/20 DOPG/eSM/Chol yielded an increase of the L_d area fraction of approximately 3.5%; see Fig. 3B.

Even though the error for the area changes when averaged over vesicle populations is large and the difference between the cases with and without cyt *c* is small, we are confident that the effect is present. The measurements on individual vesicles unequivocally show that the L_d area fraction increases in the presence of the protein. In general, measurements over vesicle populations should be always backed up by direct tests on individual vesicles. Note that if the majority of the vesicles exhibits budding during the addition of the protein, systematic

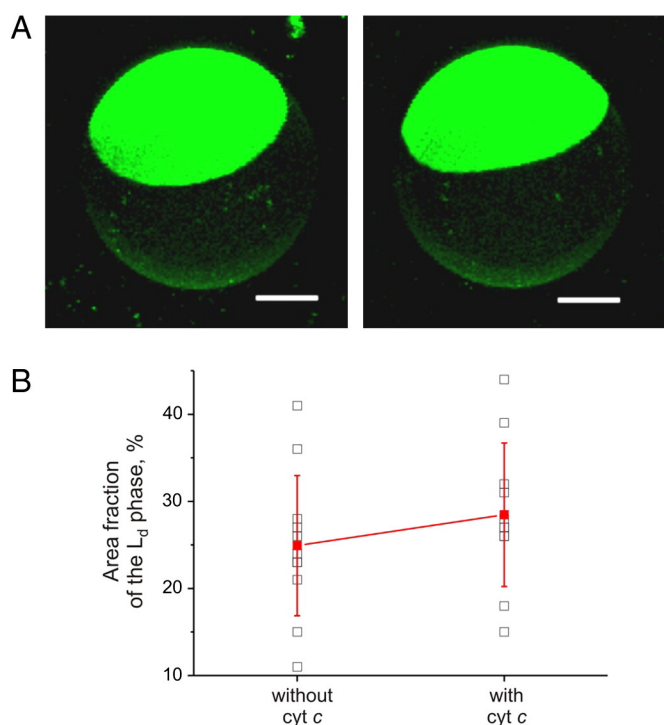


Fig. 3. Change in the domain area in 30/50/20 DOPG/eSM/Chol vesicles upon adsorption of cyt *c* at a concentration of 0.56 μM. (A) 3D projections of a vesicle before (left) and after (right) introducing cyt *c*. The membrane was labeled with DiI_{C18} which preferentially partitions into the L_d phase. Scale bars correspond to 10 μm. Upon adsorption of cyt *c*, the L_d domain area increases by approximately 5% (B) Change in the area fraction of the L_d domains measured on two vesicle populations before and after the addition of cyt *c* (open squares). The average values (solid squares) are also given. The error bars represent standard deviations.

shifts in the membrane composition of the vesicles are expected, affecting the final distribution of the data as obtained for vesicle populations.

The above results imply that upon interaction and binding of cyt *c* to multicomponent lipid membranes containing charged lipids, apart from demixing, the protein causes redistribution of lipids. Apparently, the bound protein attracts more charged lipids to the liquid disordered domains where it predominantly binds (as we will see in the next section) leading to an increase of the area of the L_d domains.

3.4. Preferential partitioning of cyt *c* between liquid ordered and liquid disordered domains

To find out whether cyt *c* exhibits preferences to raft-like domains in cells or rather tends to avoid them, we quantitatively characterized the partitioning of the protein between liquid-ordered and liquid-disordered domains in vesicles with compositions belonging to the region of coexistence of these two fluid phases. The L_o domains were identified using the fluorescent dye DSPE-PEG2000-CF, which partitions preferentially into the L_o phase.

To resolve the preferential adsorption of cyt *c*, we labeled the protein with Alexa Fluor 633. No overlap in the spectra with the lipid dye was observed in the detection ranges used in this work. The final protein concentration of the labeled analog was determined from absorbance measurements; see Fig. S3. We did not observe an effect of the fluorescent label on the adsorption behavior of the protein as judged by the change in the domain area fractions.

To examine the preferential partitioning of cyt *c* between the L_d and L_o phases, we chose the same three membrane compositions considered in the previous section. After preparing the GUVs, the solution of the labeled cyt *c* was added drop-wise reaching a final concentration of 0.56 μM. After allowing for 30 min equilibration in the observation

chamber, the vesicles were examined with confocal microscopy. Fig. 4 shows cross section images of a vesicle with domains in the presence of the protein. Direct observation of the images suggests that cyt *c* preferentially partitions into the L_d phase, i.e. the DOPG-rich domains. This behavior is expected as positively charged cyt *c* would preferentially interact with the more negatively charged L_d domains. Our data are also in agreement with another qualitative study reporting preferential partitioning of cyt *c* in cardiolipin-rich domains [7]. In addition, our measurements also provide evidence for weak partitioning of cyt *c* into the L_o domains; see Fig. 4B and the following paragraph, which reflects the fraction of charged lipids present in the raft-like L_o phase.

The partitioning of cyt *c* between L_d and L_o phases was quantitatively characterized by analyzing the intensity profiles of the fluorescence signal of the protein in the confocal images of GUVs. The image analysis was performed using an in-house-written program in Matlab, which traces the vesicle contour by a least-squares algorithm [54]. The fluorescence intensity along the membrane was extracted from the image after changing from Cartesian to polar coordinates (r, θ); see inset in Fig. 5B. The L_d and L_o phases were identified from the angular intensity profile of the signal from the dye DSPE-PEG2000-CF, which partitions preferentially into the L_o phase; see Fig. 5A. Then, the signal in the red channel, i.e. the intensity from cyt *c* only, along the radial direction r was averaged over the polar angle θ individually for the L_d and the L_o phases; see Fig. 5B.

The data was analyzed in the following way. At identical settings of the microscope, we measured the background signal from a sample containing the pure buffer and subtracted it from the intensity profile of the vesicle. We found that the signal inside the vesicle was higher than the background value (see Supporting Information), suggesting cyt *c* permeating the membranes as we will discuss further below. The signal from cyt *c* adsorbed on the membrane was obtained after subtracting the background, which can be well fitted by the sum of a Gaussian distribution and a Gauss error function with 0.5 μm width. The latter is justified by a diffraction-like broadening of the signal as described by the point spread function, which can be approximated with a Gaussian profile. Therefore, the total intensity signal as measured in Fig. 5B can be represented as a superposition of a Gaussian distribution, a Gauss error function, and a constant background value; see dashed and solid lines in Fig. 5B.

We then find the areas of the Gaussian profiles A_{L_d} and A_{L_o} for cyt *c* adsorbed on the L_d and the L_o phases, respectively. Their ratio, $P_{L_d/L_o} = A_{L_d}/A_{L_o}$, determines the partitioning ratio of cyt *c* between the two phases.

Note that the above analysis does not require knowledge on whether the protein permeates the membrane of the vesicles. Upon permeation, for example caused by pore formation in the membrane [55], the protein adsorption–desorption equilibrium will be established also at the internal leaflet of the vesicle membrane. The adsorbed protein will redistribute between the two fluid phases and even though this might affect the absolute value of the intensity at the membrane in the different phases, their ratio will not be affected. Furthermore, as we mentioned above, the domains in the opposite leaflets were in registration.

For each of the three compositions, 20/60/20, 30/50/20 and 40/40/20, we analyzed 79, 90 and 43 vesicles respectively. Fig. 6 summarizes the results for the partitioning ratio P_{L_d/L_o} of cyt *c* between the two phases for the three different lipid compositions belonging to the two-fluid-phase coexistence region. For all compositions, P_{L_d/L_o} is larger than one indicating that the protein favors adsorption to the L_d domains which contain a large molar fraction of negatively charged DOPG. Another important outcome of our measurements is that the partitioning ratio does not change significantly with variation in the overall membrane composition. On average, the ratio $P_{L_d/L_o} \approx 4.42 \pm 1.15$, i.e. the concentration of the adsorbed cyt *c* in the L_d domain is more than four-fold larger than that of cyt *c* adsorbing to the raft-like L_o phases. Because the PEG dye could, in principle, affect the partitioning of cyt *c*,

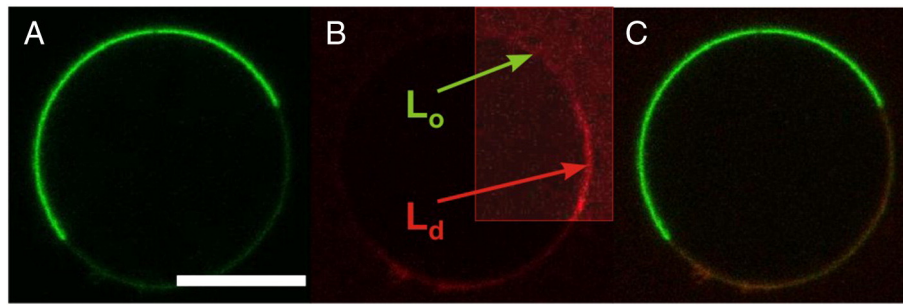


Fig. 4. Cytochrome *c* preferentially adsorbs to the L_d phase domain as demonstrated by cross section confocal images of a GUV composed of 40/40/20 DOPG/eSM/Chol, with fluorescent signals from DSPE-PEG2000-CF (green) partitioning predominantly in the L_o phase (A), labeled cyt *c* (red) partitioning predominantly in the L_d phase (B), and their merged image (C). The upper right part of the image in panel (B) is enhanced to show the stronger preference of the protein to the L_d phase and weak fluorescence in the vesicle exterior resulting from free cyt *c*. The scale bar corresponds to 10 μm .

we examined a few vesicles, which were not labeled with DSPE-PEG2000-CF. The partitioning ratio was found to be $P_{L_d/L_o} = 3.95 \pm 0.4$, which is similar to that in labeled vesicles. We thus conclude that the PEG label has no significant effect on the partitioning of cyt *c*. We assume that cyt *c* predominantly interacts with the oppositely charged DOPG. This was confirmed by tests performed on phase separated vesicles where DOPG was replaced by dioleoylphosphatidylcholine (DOPC). On vesicles made of DOPC/eSM/Chol 30/50/20 no detectable

adsorption of the protein was observed; see Fig. S4 in the Supporting Information. If cyt *c* interacted only with DOPG, the concentration of DOPG in the L_d phase would be 4.42 times larger than in the L_o phase for all three membrane compositions explored. In the considerations above, we have tacitly assumed that the adsorption interaction of cyt *c* with DOPG in the L_o phase follows the same linear law of mass action as that in the L_d phase and that the adsorption to the L_d phase has not reached saturation.

Inspection of the phase diagram in Fig. 6 shows that the mole fraction X of DOPG satisfies $0.1 < X < 0.6$ for all compositions within the fluid–fluid coexistence region obtained here. Therefore, this coexistence region can contain tie lines with two end points, a and b , that are characterized by $X_a/X_b = 4.4$, i.e., by the partitioning ratio P_{L_d/L_o} of DOPG for the two coexisting fluid phases as deduced from the fluorescence data. Any such tie line must not cross the end tie line that provides the boundary between the fluid–fluid and the three-phase coexistence region. In Fig. 6, we have included such a tie line (broken purple line) that is close to all three lipid compositions, for which the partitioning ratio was found to be essentially constant. Within the measurement error, the area fractions of the L_d and L_o domains as deduced from Fig. 3B roughly correspond to the requirement as set by the lever rule, in such a way that the area of the L_d domain is smaller than the area of the L_o domain. The angle between this tentative tie line and the DOPG/eSM side of the Gibbs triangle is relatively small and about 13° . However, any conclusions we can currently draw about the inclination of the tie

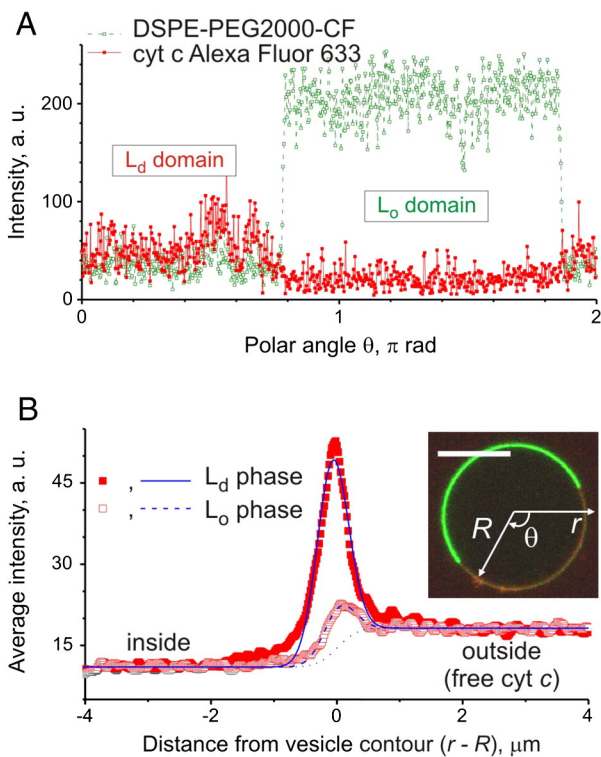


Fig. 5. Fluorescence intensity analysis of the partitioning of cyt *c* in the L_o and L_d domains of a vesicle composed of 40/40/20 DOPG/eSM/Chol (same vesicle as in Fig. 4). (A) Angular dependencies of the fluorescent intensity along the vesicle contour for cyt *c* (red) and DSPE-PEG2000-CF (green). The green signal is used to allocate the regions of the membrane in L_o or L_d phases. (B) Fluorescence intensity of cyt *c* averaged over the polar angle for the L_d phase (solid squares) and L_o phase (open squares). The dotted line represents the fit of the signal inside and outside the vesicle to a sum of a Gaussian error function and a constant; see text for details. The solid and dashed lines are fits of the experimental data for the L_d and L_o phases, respectively. These fits represent sums of a Gaussian distribution for cyt *c* adsorbed to the membrane, a superposition of Gaussian error function and a constant for the free cyt *c* in the external and the internal solution. The inset shows an image of the analyzed vesicle with the polar coordinates indicated. For this particular vesicle, we obtain the partitioning ratio $P_{L_d/L_o} = 2.41$.

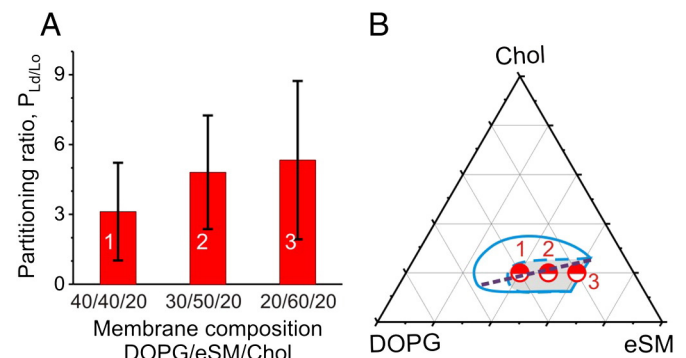


Fig. 6. Partitioning of cyt *c* in vesicles with L_d and L_o domains. (A) The dependence of cyt *c* partitioning between L_d and L_o phases as given by the intensity ratio of the cyt *c* signal in the L_d and L_o domains for the different compositions. The error bars represent standard deviation. The numbers on the bars correspond to the numbers indicating the different membrane compositions in the ternary phase diagram in (B). (B) Gibbs triangle with schematically indicated regions of coexistence of L_d and L_o phases in the presence of cyt *c* (solid blue curve) and absence of cyt *c* (dashed blue curve) as shown in Fig. 2. The dashed purple line describes a possible tie line in the two-fluid phase coexistence region in the presence of cyt *c*; see text for details.

line are highly speculative in view of the poor precision of the phase boundaries of the two-fluid phase coexistence region that we have sketched in Figs. 2 and 6.

3.5. Cyt *c* permeation through the membrane

From the confocal images of some of the vesicles, we visually observed weak fluorescence from cyt *c* both in the vesicle exterior and in the vesicle interior (see Fig. 4B). To quantify the signal inside the vesicle and to find out whether it arises from cyt *c* present in the vesicle interior or representing some background noise, we also measured the fluorescence intensity of a sample containing only the buffer and using identical settings of the laser intensity and the image acquisition. This background noise was found lower than the intensity in the vesicle interior for all images. This suggests that in all cases cyt *c* has permeated the membrane, i.e., the vesicles have leaked, however to a different degree.

To determine the degree of leakage, we performed the following analysis. The background noise (a constant estimated from the measurement with buffer only) was subtracted from the measured intensity profiles. We then compared the fluorescence intensities measured outside the vesicle, I_{ex} , and inside the vesicle, I_{in} , far from the vesicle membrane; see Fig. 7A. The intensity reflecting the concentration of free cyt *c* outside the vesicles, I_{ex} , was approximately the same for images acquired with identical settings of the microscope. This is understandable, because the bulk concentration of cyt *c* was the same in all measurements. The degree of leakage was characterized in terms of the ratio $L \equiv I_{\text{in}}/I_{\text{ex}}$. For $L = 100\%$, the vesicles have fully leaked, while for lower values of L , partial leakage has occurred. The leakage data for vesicles with different compositions are given in Fig. 7B. Between 43 and 90 vesicles per composition were examined.

Despite the scatter in the data, some rough conclusions can be drawn. The vesicles with composition 30/50/20 DOPG/eSM/Chol exhibited the strongest leakage. About 65% of these vesicles have fully leaked, while the remaining ones exhibit partial leakage with a peak around $L = 60\%$. The majority of the vesicles from the other two compositions showed partial leakage around $L = 40\%$. The compositional dependence of the degree of leakage may suggest that the successful pore formation requires certain stoichiometry between the protein and the membrane composition, and, in particular, the fraction of the charged lipid.

Leakage of vesicles upon adsorption of cyt *c* has been observed for membranes made of phosphocholine and cardiolipin (and, in some cases, cholesterol) [55]. The leakage was ascribed to pore formation induced by negative spontaneous curvature, resulting from the adsorption of the protein, and subsequent unfolding. In reference [55] however, relatively high concentrations of the protein were used

corresponding to L/P ratios between approximately 0.1 and 2. Here, the protein concentration is much lower ($L/P = 16$), which explains the lower degree of leakage compared to that observed in [55]. Indeed, we also roughly estimated the amount of the bound protein finding that approximately 50% of the protein in solution was adsorbed to GUVs for all lipid compositions; see the Supporting Information. Very recently, the same group explored a broader range of protein concentrations [56]. However, the membrane composition was somewhat different from that studied here and the measured permeability represented the permeability of the membrane to ions and not necessarily to cyt *c*. Another difference compared to the measurements performed in reference [55] is the asymmetry between the solution enclosed in the vesicles (sucrose only) and the bathing media (salt solution), which might be an additional source of tension in the membrane arising from spontaneous curvature [57]. This asymmetry was lacking in our vesicles.

Our results on vesicle leakage combined with the finding on the strong partitioning of cyt *c* in the liquid disordered phase may imply that during apoptosis and cyt *c* release, the protein effectively destabilizes not only the mitochondrial membrane but also other charged intracellular membranes that it encounters as we discuss in more detail in the concluding section.

4. Conclusions

The phase diagram of the ternary mixture DOPG/eSM/Chol was characterized in buffered conditions. Compared to the buffer-free solution [30], we found a number of differences in the phase behavior of the membranes. The two-fluid-phase coexistence region is expanded and shifted towards higher fractions of DOPG, and a three-phase coexistence region could be identified. The addition of cyt *c* at relatively low submicromolar concentrations was shown to induce phase separation for compositions belonging to the single-fluid-phase region in the absence of the protein and, thus, to expand the two-fluid-phase coexistence region.

Under physiological conditions, cyt *c* plays an important role in the respiratory chain of eukaryotic cells and acts to transfer electrons between two transmembrane complexes in the inner membrane of mitochondria. During this process, the positively charged cyt *c* stays in continuous contact with anionic lipids [58]. In addition, cyt *c* also plays a role in apoptosis, which

Involves movement of pro-apoptotic proteins from the cytosol to the mitochondrial membranes [59,60]. Several studies have indicated that these non-residential proteins induce cyt *c* release from the mitochondria by channel formation or activation of permeability transition pores [61–63]. The resulting concentrations of cytosolic cyt *c* in rat heart were estimated to be on the order of 10 μM [64]. As argued in [55], cyt *c* may even orchestrate its own release into the cytosol by forming membrane pores.

Indeed, we observed these processes already for cyt *c* concentrations below 1 μM , i.e., for concentrations that are much smaller than the estimated concentrations of cytosolic cyt *c* during apoptosis. Therefore, the re-adsorption of cytosolic cyt *c* onto mitochondrial or non-mitochondrial membranes may lead to lipid redistribution and domain formation within these membranes as well. In this way, cyt *c* can generate additional perturbations of the signal transduction and metabolic pathways in the cell, perturbations that are likely to enhance the process of apoptosis.

Acknowledgments

This study was supported by the Deutsche Forschungsgemeinschaft (DFG) via IGRTG 1524 on “Self-Assembled Soft Matter Nano-Structures at Interfaces”. YL is partially supported by the grant of the MPG-CAS Partner Group Program.

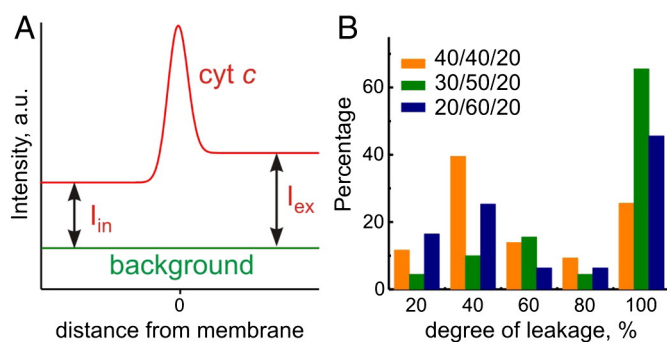


Fig. 7. Vesicle leakage. (A) Schematic illustration for the analysis on leakage: The background signal (green) as measured on samples containing buffer only is compared to the intensity profile (red). The background value is subtracted from the intensity measured inside and outside the vesicle yielding the values I_{in} and I_{ex} , respectively, as indicated in the sketch. The ratio $I_{\text{in}}/I_{\text{ex}}$ represents the degree of leakage. (B) Histogram of the degree of leakage $I_{\text{in}}/I_{\text{ex}}$ for membranes with different composition. The bin size was set to 20%.

Appendix A. Supplementary data

Supplementary data to this article can be found online at <http://dx.doi.org/10.1016/j.bbamem.2014.04.019>.

References

- [1] H.F. Lodish, A. Berk, P. Matsudaira, C.A. Kaiser, M. Krieger, M.P. Scott, S.L. Zipursky, J. E. Darnell, Molecular cell biology, 5th ed. Freeman, New York, 2004.
- [2] S. May, D. Harries, A. Ben-Shaul, Lipid demixing and protein-protein interactions in the adsorption of charged proteins on mixed membranes, *Biophys. J.* 79 (2000) 1747–1760.
- [3] E.C. Mbamala, A. Ben-Shaul, S. May, Domain formation induced by the adsorption of charged proteins on mixed lipid membranes, *Biophys. J.* 88 (2005) 1702–1714.
- [4] S. Oellerich, S. Lecomte, M. Paternostre, T. Heimburg, P. Hildebrandt, Peripheral and integral binding of cytochrome c to phospholipids vesicles, *J. Phys. Chem. B* 108 (2004) 3871–3878.
- [5] Y. Hudecek, P. Hildebrandt, D. Marsh, T. Heimburg, Spectroscopic studies of cytochrome c interaction with lipid membranes—the coupling of cytochrome c function with surface absorption and integration, *Spectroscopy of Biological Molecules: Modern Trends*, 1997, pp. 297–300.
- [6] M.J. Zuckermann, T. Heimburg, Insertion and pore formation driven by adsorption of proteins onto lipid bilayer membrane–water interfaces, *Biophys. J.* 81 (2001) 2458–2472.
- [7] P.A. Beales, C.L. Bergstrom, N. Geerts, J.T. Groves, T.K. Vanderlick, Single vesicle observations of the cardiolipin–cytochrome c interaction: induction of membrane morphology changes, *Langmuir* 27 (2011) 6107–6115.
- [8] A. Rietveld, P. Sijens, A.J. Verkleij, B. Dekruif, Interaction of cytochrome c and its precursor apocytochrome c with various phospholipids, *EMBO J.* 2 (1983) 907–913.
- [9] D.M. Haverstick, M. Glaser, Influence of proteins on the reorganization of phospholipid-bilayers into large domains, *Biophys. J.* 55 (1989) 677–682.
- [10] T. Heimburg, B. Angerstein, D. Marsh, Binding of peripheral proteins to mixed lipid membranes: effect of lipid demixing upon binding, *Biophys. J.* 76 (1999) 2575–2586.
- [11] G.P. Gorbenko, V.M. Trusova, J.G. Molotkovsky, P.K.J. Kinnunen, Cytochrome c induces lipid demixing in weakly charged phosphatidylcholine/phosphatidylglycerol model membranes as evidenced by resonance energy transfer, *Biochim. Biophys. Acta Biomembr.* 1788 (2009) 1358–1365.
- [12] K. Simons, D. Toomre, Lipid rafts and signal transduction, *Nat. Rev. Mol. Cell Biol.* 1 (2000) 31–39.
- [13] K. Simons, E. Ikonen, How cells handle cholesterol, *Science* 290 (2000) 1721–1726.
- [14] M. Edidin, The state of lipid rafts: from model membranes to cells, *Annu. Rev. Biophys. Biomol. Struct.* 32 (2003) 257–283.
- [15] T. Garofalo, R. Misasi, V. Mattei, A.M. Giammarioli, W. Malorni, G.M. Pontieri, A. Pavan, M. Soric, Association of the death-inducing signaling complex with microdomains after triggering through CD95/Fas—evidence for caspase-8-ganglioside interaction in T cells, *J. Biol. Chem.* 278 (2003) 8309–8315.
- [16] J. Fullekrug, K. Simons, Lipid rafts and apical membrane traffic, gastroenteropancreatic neuroendocrine tumor disease: molecular and cell biological aspects, 10142004. 164–169.
- [17] D. Holowka, J.A. Gosse, A.T. Hammond, X.M. Han, P. Sengupta, N.L. Smith, A. Wagenknecht-Wiesner, M. Wu, R.M. Young, B. Baird, Lipid segregation and IgE receptor signaling: a decade of progress, *Biochim. Biophys. Acta Mol. Cell Res.* 1746 (2005) 252–259.
- [18] D. Meder, M.J. Moreno, P. Verkade, W.L.C. Vaz, K. Simons, Phase coexistence and connectivity in the apical membrane of polarized epithelial cells, *Proc. Natl. Acad. Sci. U. S. A.* 103 (2006) 329–334.
- [19] P.V. Escriba, Membrane-lipid therapy: a new approach in molecular medicine, *Trends Mol. Med.* 12 (2006) 34–43.
- [20] P.V. Escriba, J.M. Gonzalez-Ros, F.M. Goni, P.K.J. Kinnunen, L. Vigh, L. Sanchez-Magraner, A.M. Fernandez, X. Busquets, I. Horvath, G. Barcelo-Coblijn, Membranes: a meeting point for lipids, proteins and therapies, *J. Cell. Mol. Med.* 12 (2008) 829–875.
- [21] S. Munro, Lipid rafts: elusive or illusive? *Cell* 115 (2003) 377–388.
- [22] R. Dimova, S. Aranda, N. Bezlyepkina, V. Nikolov, K.A. Riske, R. Lipowsky, A practical guide to giant vesicles. Probing the membrane nanoregime via optical microscopy, *J. Phys. Condens. Matter* 18 (2006) S1151–S1176.
- [23] R. Dimova, Giant vesicles: a biomimetic tool for membrane characterization, *Advances in planar lipid bilayers and liposomes*, vol. 16, Academic Press, 2012, pp. 1–50.
- [24] C. Dietrich, L.A. Bagatolli, Z.N. Volovyk, N.L. Thompson, M. Levi, K. Jacobson, E. Gratton, Lipid rafts reconstituted in model membranes, *Biophys. J.* 80 (2001) 1417–1428.
- [25] R. Lipowsky, R. Dimova, Domains in membranes and vesicles, *J. Phys. Condens. Matter* 15 (2003) S31–S45.
- [26] S.L. Veatch, S.L. Keller, Separation of liquid phases in giant vesicles of ternary mixtures of phospholipids and cholesterol, *Biophys. J.* 85 (2003) 3074–3083.
- [27] T. Baumgart, A.T. Hammond, P. Sengupta, S.T. Hess, D.A. Holowka, B.A. Baird, W.W. Webb, Large-scale fluid/fluid phase separation of proteins and lipids in giant plasma membrane vesicles, *Proc. Natl. Acad. Sci. U. S. A.* 104 (2007) 3165–3170.
- [28] S.L. Veatch, P. Cicuta, P. Sengupta, A. Honerkamp-Smith, D. Holowka, B. Baird, Critical fluctuations in plasma membrane vesicles, *ACS Chem. Biol.* 3 (2008) 287–293.
- [29] T. Baumgart, G. Hunt, E.R. Farkas, W.W. Webb, G.W. Feigenson, Fluorescence probe partitioning between L- α /L-d phases in lipid membranes, *Biochim. Biophys. Acta Biomembr.* 1768 (2007) 2182–2194.
- [30] C.C. Vequi-Suplicy, K.A. Riske, R.L. Knorr, R. Dimova, Vesicles with charged domains, *Biochim. Biophys. Acta Biomembr.* 1798 (2010) 1338–1347.
- [31] N. Shimokawa, M. Hishida, H. Seto, K. Yoshikawa, Phase separation of a mixture of charged and neutral lipids on a giant vesicle induced by small cations, *Chem. Phys. Lett.* 496 (2010) 59–63.
- [32] M.C. Blosser, J.B. Starr, C.W. Turtle, J. Ashcraft, S.L. Keller, Minimal effect of lipid charge on membrane miscibility phase behavior in three ternary systems, *Biophys. J.* 104 (2013) 2629–2638.
- [33] J. Kilkus, R. Goswami, F.D. Testai, G. Dawson, Ceramide in rafts (detergent-insoluble fraction) mediates cell death in neurotumor cell lines, *J. Neurosci. Res.* 72 (2003) 65–75.
- [34] I. Gkantiragas, B. Brugger, E. Stuvén, D. Kaloyanova, X.Y. Li, K. Lohr, F. Lottspeich, F.T. Wieland, J.B. Helms, Sphingomyelin-enriched microdomains at the Golgi complex, *Mol. Biol. Cell* 12 (2001) 1819–1833.
- [35] S. Kaushik, A.C. Massey, A.M. Cuervo, Lysosome membrane lipid microdomains: novel regulators of chaperone-mediated autophagy, *EMBO J.* 25 (2006) 3921–3933.
- [36] D. Ardail, J.P. Privat, M. Egrecharlier, C. Levrat, F. Lerme, P. Louisot, Mitochondrial contact sites—lipid-composition and dynamics, *J. Biol. Chem.* 265 (1990) 18797–18802.
- [37] A. Watts, K. Harlos, W. Maschke, D. Marsh, Control of structure and fluidity of phosphatidylglycerol bilayers by pH titration, *Biochim. Biophys. Acta* 510 (1978) 63–74.
- [38] P.W.M. van Dijck, B. de Kruijff, A.J. Verkleij, L.L.M. van Deenen, J. de Gier, Comparative studies on effects of pH and Ca^{2+} on bilayers of various negatively charged phospholipids and their mixtures with phosphatidylcholine, *Biochim. Biophys. Acta* 512 (1978) 84–96.
- [39] A.J. De Siervo, M.R.J. Salton, Biosynthesis of cardiolipin in membranes of *Micrococcus lysodeikticus*, *Biochim. Biophys. Acta* 239 (1971) 280.
- [40] S.C. Chang, P.N. Heacock, C.J. Clancey, W. Dowhan, The PEL1 gene (renamed PGS1) encodes the phosphatidylglycerophosphate synthase of *Saccharomyces cerevisiae*, *J. Biol. Chem.* 273 (1998) 9829–9836.
- [41] M.I. Angelova, D.S. Dimitrov, Liposome electroformation, *Faraday Discuss.* 81 (1986) 303–311.
- [42] A.G. Ayuyan, F.S. Cohen, Lipid peroxides promote large rafts: effects of excitation of probes in fluorescence microscopy and electrochemical reactions during vesicle formation, *Biophys. J.* 91 (2006) 2172–2183.
- [43] J. Zhao, J. Wu, H.L. Shao, F. Kong, N. Jain, G. Hunt, G. Feigenson, Phase studies of model biomembranes: macroscopic coexistence of L alpha plus L beta, with light-induced coexistence of L alpha plus Lo phases, *Biochim. Biophys. Acta Biomembr.* 1768 (2007) 2777–2786.
- [44] H. Trauble, H. Eibl, Electrostatic effects on lipid phase-transitions—membrane structure and ionic environment, *Proc. Natl. Acad. Sci. U. S. A.* 71 (1974) 214–219.
- [45] A. Pralle, P. Keller, E.L. Florin, K. Simons, J.K.H. Horber, Sphingolipid-cholesterol rafts diffuse as small entities in the plasma membrane of mammalian cells, *J. Cell Biol.* 148 (2000) 997–1007.
- [46] N. Kahya, D. Scherfeld, K. Bacia, B. Poolman, P. Schwille, Probing lipid mobility of raft-exhibiting model membranes by fluorescence correlation spectroscopy, *J. Biol. Chem.* 278 (2003) 28109–28115.
- [47] R. Lipowsky, Budding of membranes induced by intramembrane domains, *J. Phys. II* 2 (1992) 1825–1840.
- [48] A.W. Tian, B.R. Capraro, C. Esposito, T. Baumgart, Bending stiffness depends on curvature of ternary lipid mixture tubular membranes, *Biophys. J.* 97 (2009) 1636–1646.
- [49] N.F. Morales-Pennington, J. Wu, E.R. Farkas, S.L. Goh, T.M. Konyakhina, J.Y. Zheng, W.W. Webb, G.W. Feigenson, GUV preparation and imaging: minimizing artifacts, *Biochim. Biophys. Acta* 1798 (2010) 1324–1332.
- [50] M. Fidorra, A. Garcia, J.H. Ipsen, S. Hartel, L.A. Bagatolli, Lipid domains in giant unilamellar vesicles and their correspondence with equilibrium thermodynamic phases: a quantitative fluorescence microscopy imaging approach, *Biochim. Biophys. Acta Biomembr.* 1788 (2009) 2142–2149.
- [51] N. Bezlyepkina, R.S. Gracià, P. Shchelokovskyy, R. Lipowsky, R. Dimova, Phase diagram and tie-line determination for the ternary mixture DOPC/eSM/cholesterol, *Biophys. J.* 104 (2013) 1456–1464.
- [52] D. Papahadjopoulos, M. Moscarello, E.H. Eylar, T. Isac, Effects of proteins on thermotropic phase-transitions of phospholipid membranes, *Biochim. Biophys. Acta* 401 (1975) 317–335.
- [53] M.D. Collins, S.L. Keller, Tuning lipid mixtures to induce or suppress domain formation across leaflets of unsupported asymmetric bilayers, *Proc. Natl. Acad. Sci. U. S. A.* 105 (2008) 124–128.
- [54] S.T. Hess, M.V. Gudheti, M. Młodzianowski, T. Baumgart, Shape analysis of giant vesicles with fluid phase coexistence by laser scanning microscopy to determine curvature, bending elasticity, and line tension, in: A. Dopico (Ed.), *Methods in membrane lipids*, vol. 400, Humana Press, 2007, pp. 367–387.
- [55] C.L. Bergstrom, P.A. Beales, Y. Lv, T.K. Vanderlick, J.T. Groves, Cytochrome c causes pore formation in cardiolipin-containing membranes, *Proc. Natl. Acad. Sci. U. S. A.* 110 (2013) 6269–6274.
- [56] J. Xu, T.K. Vanderlick, P.A. Beales, Lytic and non-lytic permeabilization of cardiolipin-containing lipid bilayers induced by cytochrome c, *PLoS ONE* 8 (2013).
- [57] R. Lipowsky, Spontaneous tubulation of membranes and vesicles reveals membrane tension generated by spontaneous curvature, *Faraday Discuss.* 161 (2013) 305–331.
- [58] G.W. Pettigrew, G.R. Moore, *Cytochromes c: biological aspects*, Springer-Verlag, Berlin, New York, 1987.
- [59] M. Capano, M. Crompton, Biphasic translocation of Bax to mitochondria, *Biochem. J.* 367 (2002) 169–178.
- [60] A.J. Garcia-Saez, I. Mingarro, E. Perez-Paya, J. Salgado, Membrane-insertion fragments of Bcl-x(L), Bax, and Bid, *Biochemistry* 43 (2004) 10930–10943.
- [61] M. Narita, S. Shimizu, T. Ito, T. Chittenden, R.J. Lutz, H. Matsuda, Y. Tsujimoto, Bax interacts with the permeability transition pore to induce permeability transition

- and cytochrome c release in isolated mitochondria, *Proc. Natl. Acad. Sci. U. S. A.* 95 (1998) 14681–14686.
- [62] T. Kuwana, M.R. Mackey, G. Perkins, M.H. Ellisman, M. Latterich, R. Schneider, D.R. Green, D.D. Newmeyer, Bid, Bax, and lipids cooperate to form supramolecular openings in the outer mitochondrial membrane, *Cell* 111 (2002) 331–342.
- [63] O. Terrones, B. Antonsson, H. Yamaguchi, H.G. Wang, J.H. Liu, R.M. Lee, A. Herrmann, G. Basanez, Lipidic pore formation by the concerted action of proapoptotic BAX and tBID, *J. Biol. Chem.* 279 (2004) 30081–30091.
- [64] V. Borutaite, A. Budriunaite, R. Morkuniene, G.C. Brown, Release of mitochondrial cytochrome c and activation of cytosolic caspases induced by myocardial ischaemia, *Biochim. Biophys. Acta (BBA) - Mol. Basis Dis.* 1537 (2001) 101–109.

SUPPORTING INFORMATION

Effect of cytochrome *c* on the phase behavior of charged multicomponent lipid membranes

Salome Patarai¹, Yonggang Liu^{1,2}, Reinhard Lipowsky¹, Rumiana Dimova^{1,*}

¹ Department of Theory and Bio-Systems, Max Planck Institute of Colloids and Interfaces, Science Park Golm, 14424 Potsdam, Germany

² State Key Laboratory of Polymer Physics and Chemistry, Changchun Institute of Applied Chemistry, Chinese Academy of Sciences, 130022 Changchun, China

* Address correspondence to Rumiana.Dimova@mpikg.mpg.de, Tel: +49 331 5679615, Fax: +49 331 5679612.

*Equilibration of the adsorption of cyt *c* to the vesicle membrane*

To evaluate whether the adsorption of cyt *c* has reached equilibrium, we measured the fluorescence intensity of cyt *c* adsorbed on a selected vesicle throughout a period of 30 min after introducing 0.56 μM cyt *c* in the chamber. From the confocal images of vesicle cross sections we extracted the fluorescence intensity of cyt *c* adsorbed to the vesicle domains separately. The fluorescence intensity signal was acquired as described in the main text. Example of the time dependence of the fluorescence intensity on a vesicle with composition 20/60/20 DOPG/eSM/Chol is shown in Fig. S1. Error bars illustrate the standard deviation from analyzing the same image several times. Our studies suggest that between 15 and 20 minutes are sufficient for the adsorption of cyt *c* to reach equilibration.

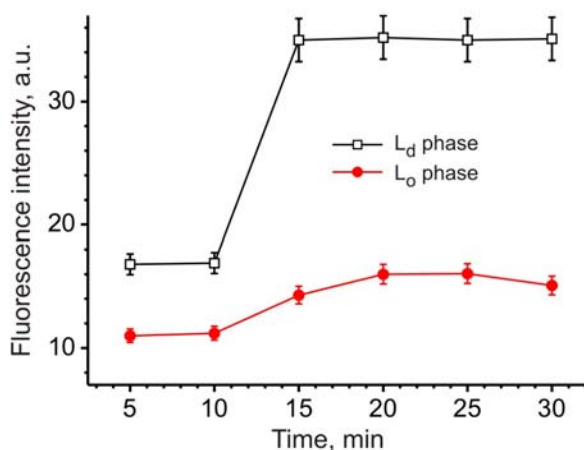


Figure S1. Time dependence of the fluorescence intensity of cyt *c* adsorbed to the L_d and L_o domains shown separately. The membrane composition was 20/60/20 DOPG/eSM/Chol. Time zero corresponds to the time at which the solution of cyt *c* was introduced in the vesicle chamber.

Bleaching of the used fluorescence dyes

We tested whether significant bleaching of the fluorescent label of *cyt c* by laser exposure occurs during the time required for capturing of consecutive images (altogether not longer than 3 minutes). The fluorescence intensity signal was acquired as described in the main text. Example of the fluorescence intensity measured on consecutive snapshots on a vesicle with composition 20/60/20 DOPG/eSM/Chol is shown in Fig. S2. Both the signal from the fluorescently labeled *cyt c* (Alexa Fluor 633) and one of the lipid dyes (DSPE-PEG200-CF) are shown. As demonstrated in Fig. S2, during the time necessary for image capturing, the signal from the fluorescently labeled *cyt c* does not change significantly. Thus, the intensity values measured for the estimate of the protein partitioning in the two phases are not influenced by bleaching of the dye. In contrast, the lipid dye bleaches significantly. However, this is not important in our case, as for the calculation of the partitioning ratios we use the fluorescence intensity of the labeled *cyt c* only.

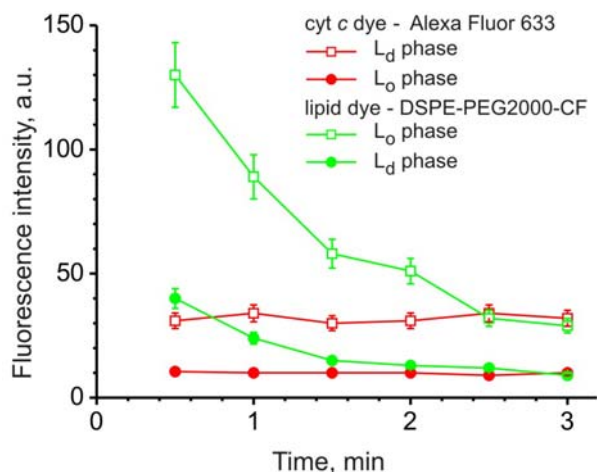


Figure S2. Bleaching of the fluorescent dyes during laser source exposure shown by intensity data for the labeled *cyt c* and lipids. The data was measured separately for the two phases. Error bars illustrate the standard deviation from analyzing the same image several times.

UV/VIS spectroscopy measurements and protein fluorescence

To resolve the preferential adsorption of *cyt c*, we considered using the fluorescence of the protein. Under the conditions used in this work, we detected weak fluorescence signal from *cyt c* in the wavelength region between 540 nm to 620 nm. However, because of the weak emission and the necessity to work at relatively high concentration of the protein (in the millimolar range), as well as the overlap of the spectrum with that of the lipid dye DSPE-PEG2000-CF, using the fluorescence of *cyt c* turned inefficient for quantitative characterization of the protein adsorption.

We measured the absorption spectra of the unlabeled yeast *cyt c* under the conditions used in this work in the wavelength range of 300 – 600 nm. On the basis of the spectra we built a calibration curve, see Fig. S3, which was used subsequently to estimate the concentration of the protein after performing the procedures for fluorescent labeling. The absorbance spectra were measured at concentrations between 1 and 5 μM in a 2 mM HEPES/1 mM EDTA buffer (pH 7.5). The absorption spectra were recorded. The molar extinction coefficient measured at 410 nm was found to be $\epsilon_{410} = 74000 \text{ M}^{-1}\text{cm}^{-1}$.

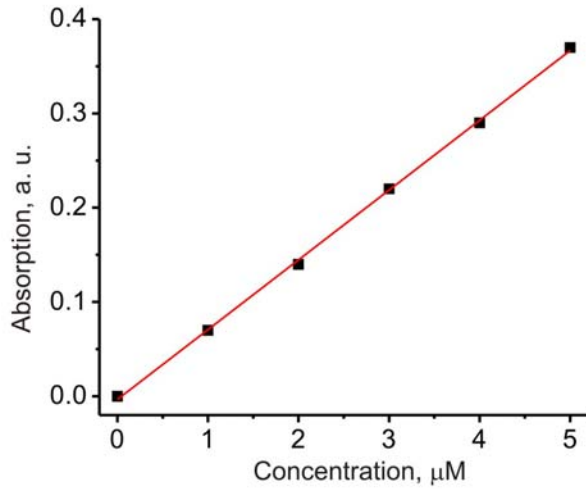


Figure S3. Absorption of yeast cyt *c* at 410 nm in 2 mM HEPES/1mM EDTA (pH 7.5) buffer at various concentrations between 1 and 5 μM . The solid line is a linear fit.

No adsorption of cyt c on DOPC/eSM/Chol membranes

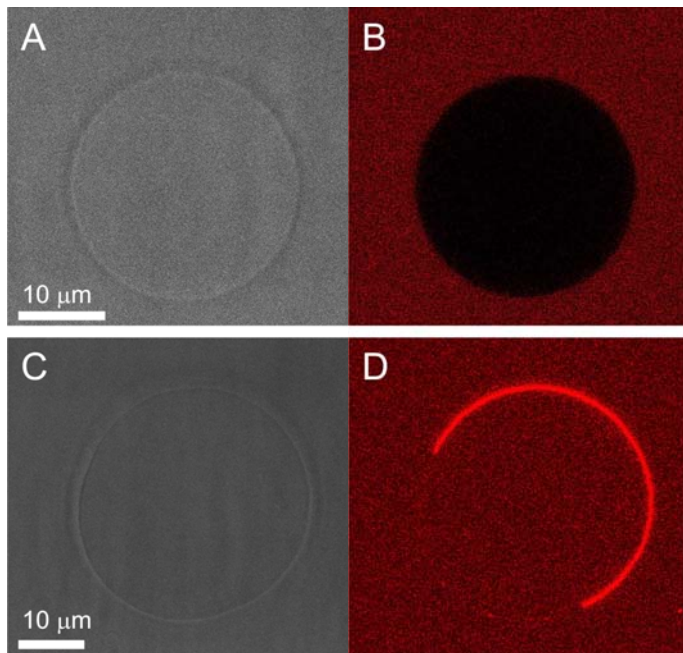


Figure S4. Evidence for no adsorption of cyt *c* to the membrane of DOPC/eSM/Chol 30/50/20 vesicles (A, B) compared to DOPG/eSM/Chol 30/50/20 vesicles (C, D): phase contrast micrographs (A, C) and confocal microscopy cross sections (B, D). Both vesicle types were incubated in 0.56 μM cyt *c* in buffer and the images were acquired at identical settings of the microscope. No protein fluorescence (red) is detected on the DOPC/eSM/Chol vesicle membrane (B). Furthermore, while the protein permeates the DOPG/eSM/Chol membranes, it does not

seem to cross the DOPC/eSM/Chol membrane as evidenced by the lack of protein fluorescence in the vesicle interior (compare the interior fluorescence with the fluorescence in the external media in B and in D).

Evaluating the relative amount of protein adsorbed to the vesicle membrane

To evaluate the amount of bound protein from the confocal images, we first measured the background intensities of samples containing the buffer or a solution of the labeled protein in buffer only. These intensities were compared with the intensity in a sample containing the vesicles and the protein in buffer. For this purpose, we made vertical (xz) scans of the samples right above the bottom glass of the observation chamber. For the vesicle sample, a scan of a vesicle-free area was taken. The microscope settings were adjusted to be exactly the same for all scans. The averaged (over x) intensities as a function from the distance from the glass (z) are displayed in Fig. S5. The peak close to the glass surface observed for the samples containing the protein corresponds to the adsorbed cyt c . At distances well above the glass ($z > 8 \mu\text{m}$), all intensities attain constant values of $I_b = 8.26 (\pm 0.10)$ for the sample with the buffer, $I_{\text{cyt}} = 35.61 (\pm 0.93)$ for the sample containing the protein solution, and $I_{\text{cyt, GUV}} = 19.94 (\pm 0.59)$ for the sample with the vesicles incubated in the protein solution. The concentration of free (not adsorbed) protein is proportional to $(I_{\text{cyt}} - I_b)$ and $(I_{\text{cyt, GUV}} - I_b)$, for the samples without and with vesicles, respectively. From the ratio of these two values, we estimate that around 57% of the total cyt c is adsorbed to 30/50/20 DOPG/eSM/Chol vesicles (Fig. S5). Similar experiments indicated that 41 % and 50 % of the total cyt c is adsorbed to 20/60/20 and 40/40/20 DOPG/eSM/Chol vesicles, respectively.

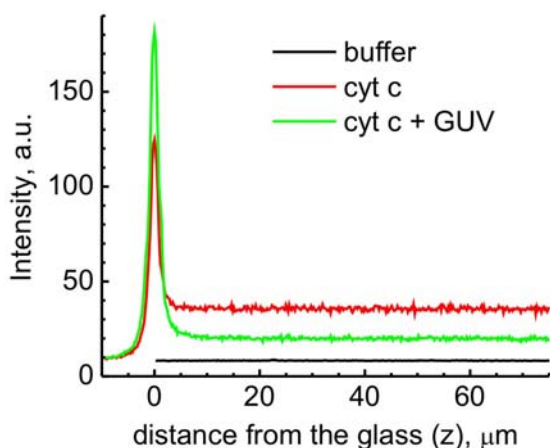


Figure S5. Averaged intensity in z directions for samples containing buffer (black curve), protein in buffer (red curve) and 30/50/20 DOPG/eSM/Chol vesicles incubated with protein in the buffer (green curve).